Modeling of Molecular Weights in Industrial Autoclave Reactors For High Pressure Polymerization of Ethylene and Ethylene-Vinyl Acetate

C. SARMORIA *and* A. BRANDOLIN*

Planta Piloto de Ingeniería Química-PLAPIQUI (UNS-CONICET)
Camino La Carrindanga km 7-8000 Bahía Blanca- Argentina

A. LÓPEZ-RODRÍGUEZ, K. S. WHITELEY, *and* B. DEL AMO FERNÁNDEZ

REPSOL, Tecnología-C/Embajadores 183
28045 Madrid-Spain

We have incorporated mass balances of monomer, radical and polymer species to a previously developed mixing model for high pressure autoclave polymerization reactors. The customary quasi steady state approximation is not used, and the method of moments is used to simplify the mass balance calculations. The resulting moment model is able to calculate conversions, average molecular weights, long chain branching and melt flow indexes at any point in the reactor. It may also calculate concentration and temperature profiles along the reactor. Results for two base cases are presented in detail. Model predictions were compared with experimental data obtained at the industrial reactor; excellent agreement was obtained. The moment balance equations are presented in a modular way so that they may be easily adapted to be used with any other mixing model for this type of reactor.

INTRODUCTION

High pressure polymerization in autoclave reactors is one of the technologies currently in use for the production of polyolefins, such as polyethylene and ethylene-vinyl acetate (EVA) copolymers. The reaction is initiated with organic peroxides at pressures between 1000 and 2000 kg/cm^2 and different temperature levels covering the range from 150 to 300°C from the top to the bottom of the reactor, which is divided into several zones connected in series following ICI technology. Typical conversion levels in these reactors are about 20%.

A wide range of polyethylenes and EVA copolymers are produced by this process. This is possible because there are different recipes to control the reactor productivity and the product molecular properties. The most common control variables are the pressure, the temperature levels, the stirring pattern, the position of the multiple injections of initiator, the particular initiator used, the location of the monomer feeds along the reactor, or the use of chain transfer agents of low molecular weight. In such a complex reactor, the use of a detailed mathematical model of the process as a design or predictive tool is preferable to making trial-and-error experiments at pilot plant or industrial scale.

This work aims at the enhancement of a computer mixing model reported by López-Rodríguez *et al.* (1) for the Repsol reactors. This mixing model took into account the kinetic mechanism, the hydrodynamics, the thermodynamics of the system—including one or two phase reaction mixture—and the control scheme applied to the reactor, making use only of the heat and initiator balances. From such a model it is possible to calculate initiator consumption, transfer agent concentration and temperature profiles along the reactor as well as melt flow indexes of final products. Good agreement between experimental and model calculated variables was previously reported (1).

Our goal is to incorporate the calculation of the higher moments of the MWD in the above mentioned mixing model. The number average molecular weight was included in the mass balance of the stirring model, but the higher moments require more sophisticated

*To whom correspondence should be addressed.

treatment. To this purpose we establish the balances of monomer, and each one of the radical and polymer species. We dispense with the quasi-steady state hypothesis for the radicals to be able to incorporate the radical inflow and outflow rates which are known to occur in the autoclave reactors. This improves the estimation of radical concentrations along the reactor, avoiding a source of inaccuracy in molecular weight calculations. The method of moments was used to simplify mass balance calculations. These moment balances could be easily adapted for use with any other mixing model. The resulting model will be referred to as the moment model in the remainder of the paper.

The moment model presented in this work, coupled with the previous mixing model, allows the prediction of temperature, concentrations, average molecular weights, and long chain branching indexes for polyethylene and EVA at any point in the reactor. The considered concentrations are those of monomer, initiators, transfer agent, global polymer and radicals. Moreover, melt flow index is now estimated as a function of the calculated molecular properties. For each one of the cells in which the mixing model divides the reactor zones, a set of at least fourteen nonlinear algebraic equations must be solved. All cells must be solved simultaneously because they are connected through internal flows. Since a typical number of cells in a reactor zone may range between 50 and 100, a large number of equations results.

Repsol Química provided basic kinetic parameter relationships and values, where the possibility of different phase operation was taken into account through an "ad hoc" correlation for the rate constant of transfer to polymer. This correlation is confidential.

In general, the moment model predictions follow the observed experimental trends, both for homopolymer and copolymer. Nevertheless, a parameter fine tuning was performed to improve the match between calculated and experimental molecular weights of polymers obtained under a wide range of operating conditions, none of which led to gel formation. A total of 15 polymers, including both polyethylene and EVA copolymers, were used for the adjusting process. The predictive capability of the adjusted moment model was checked using another set of 13 independent experimental data. The agreement was very good, within the experimental measurement error for these molecular weights. As an example, we present detailed design and kinetic information on a typical autoclave reactor used for both ethylene and ethylene-vinyl acetate polymerization.

A literature review shows that other attempts at modeling this type of reactor have been published (2–5), which present different degrees of detail. All of them proposed mixing models including polymerization rate calculations. Chan *et al.* (5) pointed out the complications of mathematical modeling of autoclave reactors: the non-ideal mixing, the existence of two phase reactions and the possibility of gel formation. They were the only authors to model molecular weights, making use of the quasi-steady state hypothesis for the radicals and allowing for gel formation.

They considered a reactor with about 40 paddles, considerably more than the number present in the Repsol reactors (1). They considered the kinetic scheme from Zabisky *et al.* (6), including the use of pseudo-constants for the copolymer. Most of the kinetic parameters used were taken from the literature. They performed a sensitivity study on some of the parameters of their mixing model, which they finally adjusted against experimental temperature profiles. They also compared model predictions with flow rates and conversion. With respect to molecular weights, they presented results on how their mixing model parameter values affected the predictions of number-average molecular weights and polydispersity. As they did not have the corresponding experimental data available, they could not compare their molecular property predictions against them. For the commercial reactor they showed normalized temperature profiles only, while pointing out that the actual kinetic constants and design parameters used had to remain confidential.

The model presented in this work differs from the one in Chan *et al.* (5) in several aspects. We use a different mixing model, where only continuous stirred tank reactors connected radially and longitudinally are considered (1). The kinetic scheme that we use is simpler, as detailed later in the paper. On the other hand, we do not apply the pseudo steady state approximation for the radicals. When the moment model presented in this work is coupled with the previous mixing model, it is possible to calculate temperature, concentrations, number-, weight- and z-average molecular weights, long chain branching index and melt flow index for polyethylene and EVA at any point in the reactor. We are not concerned with the mixing model parameters, and focus more on the simulation results.

In this work we show all details for example calculations and normalized results for the industrial reactors, in an approach similar to that of Chan *et al.* (5). The kinetic data reported for our examples arise from the parameter adjustment performed using experimental data.

REACTOR MODEL

Mixing Model

The mixing model was previously published (1), and its predictions agree well with the performance of the considered industrial reactors. It assumes axial symmetry and uses geometric data such as reactor length, diameter, number, size and location of paddles, initiator injection points, number and location of gas inlets. The reactor is divided into zones, and each reaction zone is divided into several cells, as shown in *Fig. 1*. Each cell is assumed to be perfectly stirred, and two phase reaction is allowed within it. Cells may

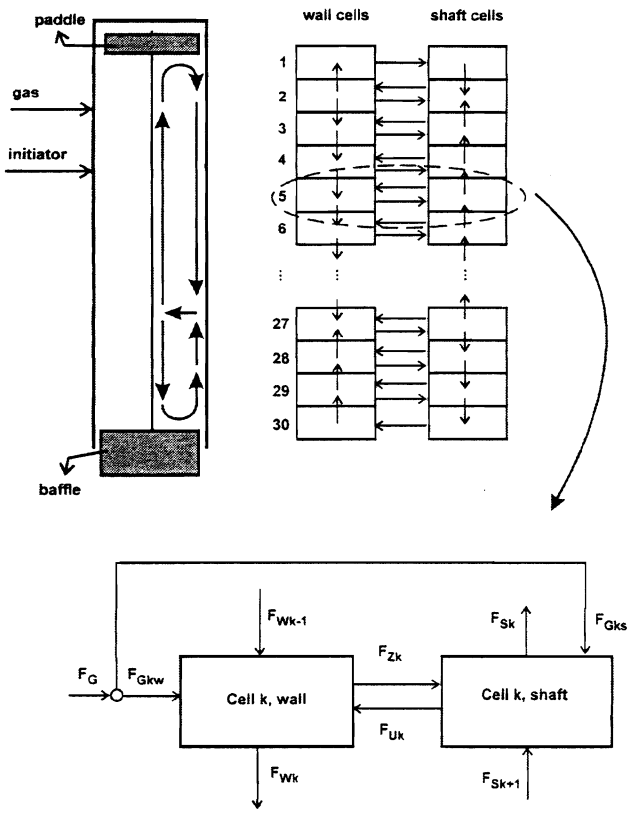

Fig. 1. Schematic representation of a single zone in an autoclave reactor, and its description in terms of interconnected cells.

exchange heat and mass with each other. The blown up detail in *Fig. 1* shows a scheme of the possible axial and radial volumetric flux pattern between generic cells. This pattern considers a cold feed (F_G) which may be located at any level in the reactor coinciding with a given "k" cell. This feed gets distributed between the wall (F_{Gkw}) and the shaft (F_{Gks}) by diffusion because of reactor stirring. It also considers wall and shaft axial fluxes (F_{Wk}, F_{Sk}), and radial fluxes between wall and shaft cells (F_{Zk}, F_{Uk}). The magnitude and direction of the inner circulating flows that appear were already determined experimentally as reported in (1). Most of the heat of polymerization is assumed to be absorbed by the cold ethylene feeds. The polymerization rate was calculated at each cell by means of a combination of the usual quasi-steady state expression of the overall polymerization rates with an empirical correlation which relates monomer concentration and the rates of propagation and termination. The initiator injection rates were determined by trial-and-error through a PID control equation, until temperature at the set location reached the desired value.

Several mixing model results are used as data by the moment model, such as the inner circulating flows, the radial and axial profiles of temperature and those of concentration of both the initiators and the transfer agents.

Moment Model

As a first step, the monomer, radical and polymer mass balances in the reactive phase must be established. Each radical and polymer molecule is characterized by its number of long branches "i" and by its length "x". Length is measured as number of monomer units in the chain. In this way $P_i(x)$ and $R_i(x)$ symbolize each of the polymer and radical species in the reactor. The index "i" must be any integer between 1 and infinity, while "x" may be any non-negative integer. This level of detail allows the description of the distributions in length and branch number of the polymer. Since an infinite number of polymer and radical species is possible, the complete set of balance equations is infinitely large. To overcome this difficulty, we have made use of double moment definitions. After applying them to the balance equations together with a closure technique a finite set of equations results. Solution of this set allows the calculation of average molecular weights and long-chain branching indexes.

In what follows we describe the kinetic mechanism and the mass balances that are used in the moment model. We also give the details on the application of the moment technique in order to obtain the moment balances.

Kinetic Mechanism

The following basic reactions *Eqs 1–7*, considered to be important in the polymerization of ethylene alone or in presence of vinyl acetate (6, 7), are included in the model:

Peroxide Initiation

$$I_j \xrightarrow{f_j k_{cj}} 2R_1(0) \quad j = 1..NIT \tag{1}$$

Propagation

$$R_i(x) + M \xrightarrow{k_p} R_i(x+1) \tag{2}$$

Termination by Combination

$$R_i(x) + R_j(y) \xrightarrow{k_{tc}} P_{i+j-1}(x+y) \tag{3}$$

Thermal Degradation (scission)

$$R_i(x) \xrightarrow{k_{tdt}} P_i(x) + R_1(0) \tag{4}$$

Chain Transfer to Polymer

$$R_i(x) + P_j(y) \xrightarrow{yk_{trp}} P_i(x) + R_{j+1}(y) \tag{5}$$

Chain Transfer to Solvent

$$R_i(x) + S_j \xrightarrow{k_{trs_j}} P_i(x) + R_1(0) \quad j = 1..NST \tag{6}$$

Chain Transfer to Monomer

$$R_i(x) + VA \xrightarrow{k_{trm}} P_i(x) + R_1(1) \tag{7}$$

We assume that the selected mechanism is able to describe ethylene polymerization as well as ethylene copolymerization with vinyl acetate. In the above equations "*M*" symbolizes the sum of all monomers present (either ethylene alone or ethylene plus vinyl acetate (VA)). Please note that chain transfer to monomer is only important for VA. No specific balance for vinyl acetate needs to be considered because the associated transfer constant that we use is given per %VA w/w fed to the reactor; a balance of global monomer (*M*) is enough. The values for the kinetic constants and their relationships result from a combination of sources: open literature, peroxide manufacturers and in-house values, followed by a parameter adjustment for the remaining values as described in the sections that follow.

Mass Balances

Equations 8 to *10* describe the non-steady-state mass balances for all the species present at each one of the cells in which the reactors are divided according to the mixing model (see *Fig. 1*). The set of equations may be reduced to the steady state case by equating the right hand side of each equation to zero. In what follows, please refer to the list of nomenclature at the end of the paper.

Global Monomer at Cell "*k*" (k = ks or kw, with ks = 1, 2,...*Ncell*/2 and kw = 1, 2,...*Ncell*/2)

$$\frac{d\{[M]_k V_k}{dt} = \sum_{i=1}^{Nin_k} [M]_{in_i} F_{Vin_i} - \sum_{i=1}^{Nout_k} [M]_k F_{Vout_i} - k_{p_k}[M]_k[Ra]_k V_k - k_{trm_k}[VA]([Ra]_k - [R_1(0)]_k)V_k \quad (8)$$

Radicals $R_i(x)$ (i = 1, 2, ...∞; x = 0, 1, 2, ...∞) at Cell "*k*" (k = ks or kw, with ks = 1, 2,...*Ncell*/2 and kw = 1, 2,...*Ncell*/2)

$$\frac{d\{[R_i(x)]_k V_k}{dt} = \sum_{i=1}^{Nin_k} [R_i(x)]_{in_i} F_{Vin_i} - \sum_{i=1}^{Nout_k} [R_i(x)]_k F_{Vout_i} + \sum_{j=1}^{NIT} 2 f_j k_{cl_k}[I_j]_k \delta_{i1}\delta_{x0} V_k - k_{p_k}[M]_k[R_i(x)]_k V_k + k_{p_k}[M]_k[R_i(x-1)]_k V_k - 2k_{tc_k}[R_i(x)]_k[Ra]_k V_k - k_{tdt_k}[R_i(x)]_k(1-\delta_{x0})V_k + k_{tdt_k}([Ra]_k - [R_1(0)]_k)\delta_{i1}\delta_{x0} V_k - k_{trp_k}[R_i(x)]_k(1-\delta_{x0})\sum_{j=1}^{\infty}\sum_{y=1}^{\infty} y[P_j(y)]V_k + k_{trp_k}([Ra]_k - [R_1(0)]_k)x[P_{i-1}(x)]_k V_k - \sum_{j=1}^{NST} k_{trs_{j_k}}[R_i(x)]_k(1-\delta_{x0})[S_j]_k V_k + \sum_{j=1}^{NST} k_{trs_{j_k}}([Ra]_k - [R_1(0)]_k)[S_j]_k \delta_{i1}\delta_{x0} V_k - k_{trm_k}[R_i(x)]_k(1-\delta_{x0})[VA]V_k + k_{trm_k}([Ra]_k - [R_1(0)]_k)\delta_{i1}\delta_{x1}[VA]V_k \quad (9)$$

Polymer $P_i(x)$ (i = 1, 2, ...∞; x = 1, 2, ...∞) at cell "*k*" (k = ks or kw, with ks = 1, 2,...*Ncell*/2 and kw = 1, 2,...*Ncell*/2)

$$\frac{d\{[P_i(x)]_k V_k}{dt} = \sum_{i=1}^{Nin_k} [P_i(x)]_{in_i} F_{Vin_i} - \sum_{i=1}^{Nout_k} [P_i(x)]_k F_{Vout_i} + k_{tc_k}\sum_{j=1}^{i}\sum_{y=0}^{x}[R_j(y)]_k[R_{i-j+1}(x-y)]_k V_k + k_{tdt_k}[R_i(x)]_k V_k + k_{trp_k}[R_i(x)]_k\sum_{j=1}^{\infty}\sum_{y=1}^{\infty} y[P_j(y)]_k V_k - k_{trp_k}([Ra]_k - [R_1(0)]_k)xP_i(x)_k V_k + \sum_{j=1}^{NST} k_{trs_{j_k}}[R_i(x)]_k[S_j]_k V_k + k_{trm_k}[R_i(x)]_k[VA]V_k \quad (10)$$

As explained above, the mass balance equations are infinite in number due to the infinite possibilities of combinations of branches and monomer units to form a polymer or radical molecule. To solve such a mathematical problem we make use of the moment technique (8, 9) as described below.

Moment Equations

The following double moments for the radical and polymer distributions are defined (*Eqs 11* and *12*). The first index corresponds to the branch distribution while the second one corresponds to the length distribution.

m^{th}, n^{th} Radical Moment

$$\lambda_{m,n} = \sum_{i=1}^{\infty} i^m \sum_{x=0}^{\infty} x^n r_i(x) \quad (11)$$

m^{th}, n^{th} Polymer Moment

$$\mu_{m,n} = \sum_{i=1}^{\infty} i^m \sum_{x=1}^{\infty} x^n p_i(x) \quad (12)$$

To obtain the moment balance equations for radicals, both sides of *Eq 9* must be multiplied by $\sum_{i=1}^{\infty} i^m \sum_{x=0}^{\infty} x^n$. Similarly, to obtain the moment balance equations for the polymer, both sides of *Eq 10* must be multiplied by $\sum_{i=1}^{\infty} i^m \sum_{x=1}^{\infty} x^n$. Finally, *Eqs 13* and *14* result after some tedious mathematical work consisting of rearranging terms until they are expressed as functions of the moment definitions.

Radical moment $\lambda_{m,n}$ (m = 0,1; n = 0, 1, 2) at cell "*k*" (k = ks or kw, with ks = 1, 2,...*Ncell*/2 and kw = 1, 2,...*Ncell*/2)

$$\frac{d\{\lambda_{m,n_k} V_k\}}{dt} =$$
$$\sum_{i=1}^{Nin_k} \lambda_{m,n_{in_i}} F_{Vin_i} - \sum_{i=1}^{Nout_k} \lambda_{m,n_k} F_{Vout_i}$$
$$+ \sum_{j=1}^{NIT} 2 f_j k_{cj_k} [I_j]_k \delta_{n,0} V_k$$
$$- k_{p_k} [M]_k \lambda_{m,n_k} V_k + k_{p_k} [M]_k \sum_{j=0}^{n} \binom{n}{j} \lambda_{m,j_k} V_k$$
$$- 2 k_{tc_k} \lambda_{m,n_k} \lambda_{0,0_k} V_k$$
$$- k_{tdt_k} (\lambda_{m,n_k} - [R_1(0)]_k) V_k$$
$$+ k_{tdt_k} (\lambda_{0,0_k} - [R_1(0)]_k) \delta_{n,0} V_k$$
$$- k_{trp_k} (\lambda_{m,n_k} - [R_1(0)]_k) \mu_{0,1} V_k$$
$$+ k_{trp_k} (\lambda_{0,0_k} - [R_1(0)]_k) \sum_{j=0}^{m} \binom{m}{j} \mu_{j,n+1_k} V_k$$
$$- \sum_{j=1}^{NST} k_{trs_{j_k}} (\lambda_{m,n_k} - [R_1(0)]_k)[S_j]_k V_k$$
$$+ \sum_{j=1}^{NST} k_{trs_{j_k}} (\lambda_{0,0_k} - [R_1(0)]_k)[S_j]_k \delta_{n,0} V_k$$
$$- k_{trm_k} (\lambda_{m,n_k} - [R_1(0)]_k)[VA] V_k$$
$$+ k_{trm_k} (\lambda_{0,0_k} - [R_1(0)]_k)[VA] V_k \quad (13)$$

Polymer moment $\mu_{m,n}$ ($m = 0,1$; $n = 0, 1, 2$) at cell "k" ($k = ks$ or kw, with $ks = 1, 2,...Ncell/2$ and $kw = 1, 2,...Ncell/2$)

$$\frac{d\{\mu_{m,n_k} V_k\}}{dt} =$$
$$\sum_{i=1}^{Nin_k} \mu_{m,n_{in_i}} F_{Vin_i} - \sum_{i=1}^{Nout_k} \mu_{m,n_k} F_{Vout_i}$$
$$+ k_{tc_k} \sum_{i=0}^{n} \binom{n}{i} \sum_{l=0}^{m} \binom{m}{l} \sum_{j=0}^{l} \binom{l}{j} (-1)^{l-j} \lambda_{j,i_k} \lambda_{m-l,n-i_k} V_k$$
$$+ k_{tdt_k} (\lambda_{m,n_k} - [R_1(0)]_k) V_k$$
$$+ k_{trp_k} (\lambda_{m,n_k} - [R_1(0)]_k) \mu_{0,1_k} V_k$$
$$- k_{trp_k} (\lambda_{0,0_k} - [R_1(0)]_k) \mu_{m,n+1_k} V_k$$
$$+ \sum_{j=1}^{NST} k_{trs_{j_k}} (\lambda_{m,n_k} - [R_1(0)]_k)[S_j]_k V_k$$
$$+ k_{trm_k} (\lambda_{m,n_k} - [R_1(0)]_k)[VA] V_k \quad (14)$$

It should be noted that $\mu_{m,n+1}$ appears in the balance of $\mu_{m,n}$. This happens because transfer to polymer is assumed to be proportional to the number of monomer units in the polymer molecule rather than to the molar concentration of polymer. Because of this, when solving up to the second moment for the polymer length the third moment in length (*Eq 15*) must be estimated. In this work we used as estimation the geometric mean between the third moment of a log-normal distribution and the equivalent moment of a Γ-distribution (6). We selected this particular estimation on the basis of comparison of the z-average degree of polymerization calculated using this approximation and experimental values corresponding to the present reactors, following the procedure proposed in reference (6).

$$\mu_{m,3} = \left(\frac{\mu_{m,2}}{\mu_{m,1}}\right)^2 \sqrt{2\mu_{m,2}\,\mu_{m,0} - (\mu_{m,1})^2}, \quad m = 0, 1 \quad (15)$$

Calculated Properties

It is interesting to note the physical meaning of some of the moment definitions (10). For example the 0th, 0th moments $\left(\lambda_{0,0} = \sum_{i=1}^{\infty}\sum_{x=0}^{\infty} r_i(x),\ \mu_{0,0} = \sum_{i=1}^{\infty}\sum_{x=1}^{\infty} p_i(x)\right)$ determine the global molar concentrations of radicals and polymer. The 0th, 1st moments $\left(\lambda_{0,1} = \sum_{i=1}^{\infty}\sum_{x=0}^{\infty} x r_i(x);\ \mu_{0,1} = \sum_{i=1}^{\infty}\sum_{x=1}^{\infty} x p_i(x)\right)$ correspond to the molar concentration of monomer in radicals and polymer. Finally, the 1st, 0th moments describe the long-chain branching concentration in radicals and polymer $\left(\lambda_{1,0} = \sum_{i=1}^{\infty} i \sum_{x=0}^{\infty} r_i(x);\ \mu_{1,0} = \sum_{i=1}^{\infty} i \sum_{x=1}^{\infty} p_i(x)\right)$.

Using these definitions, it is possible to express average molecular weights as functions of moments, as follows (*Eqs 16–18*):

Number-average molecular weight

$$Mn = \frac{\mu_{0,1} + \lambda_{0,1}}{\mu_{0,0} + \lambda_{0,0}} \overline{M}_{mon} \quad (16)$$

Weight-average molecular weight

$$Mw = \frac{\mu_{0,2} + \lambda_{0,2}}{\mu_{0,1} + \lambda_{0,1}} \overline{M}_{mon} \quad (17)$$

z-average molecular weight

$$Mz = \frac{\mu_{0,3} + \lambda_{0,3}}{\mu_{0,2} + \lambda_{0,2}} \overline{M}_{mon} \quad (18)$$

Similarly, the number-average long-chain branching index may be calculated as (*Eq 19*):
Long-Chain Branching every 1000 C

$$LCB = 500 \frac{\mu_{1,0} + \lambda_{1,0}}{\mu_{0,0} + \lambda_{0,0}} \frac{\overline{M}_{mon}}{M_n} = 500 \frac{\mu_{1,0} + \lambda_{1,0}}{\mu_{0,1} + \lambda_{0,1}} \quad (19)$$

In the above equation, the ratio of the 1st, 0th moment to the 0th, 0th moment measures branches per macromolecule. In order to express LCB in branches every 1000C we multiply by $500 \frac{\overline{M}_{mon}}{Mn}$, which is the weight of a chain containing 1000 C atoms.

In this work we update the empirical correlations used in (1) to calculate the melt flow index (MFI). For this purpose we correlated experimental data on MFI with molecular properties such as *Mn*, *Mw*, and *Mz*. Different correlations were found for polyethylenes

and for EVA copolymers. For polyethylene the best correlation found for MFI depends only on *Mn*, while for the EVA copolymers it depends on *Mn*, *Mw* and the proportion of vinyl acetate in the feed. The correlation coefficients were found using experimental data on MFI, *Mn* and *Mw*. The calculated values of MFI reported in this work were evaluated using calculated values of *Mn* and *Mw*.

MATHEMATICAL MODEL RESOLUTION

In order to calculate number, weight and z-average degrees of polymerization as well as number-average long chain branching it is necessary to solve the moment balances up to the first moment in number of branches and up to the second moment in length. In such a case, the resulting set of equations consists of monomer balance (*Eq 8*), balance for $R_1(0)$ (*Eq 9* for $i = 1$, $x = 0$), moment balances (*Eqs 13* and *14*) and the truncation equation (*Eq 15*) at each cell for a given reactor section. All cells must be solved simultaneously because they are connected through internal flows. For the case in which the cell volumes remain constant, the maximum number of equations to be solved at a particular zone is given by *Eq 20*:

$$N_{eq} = 14\ Ncell \tag{20}$$

In the steady-state case, the proposed model requires the solution of a system of ill-conditioned nonlinear algebraic equations. Another way to obtain the stationary solution is solving the differential equation system for the non-steady state case, beginning from an arbitrary initial point until the stationary operation point is reached. Following this last approach the system is solved by means of a predictor-corrector integrator (11). The corresponding computer program, implemented in Fortran code, required between 20 min and 5 h of CPU time in a PC Pentium 160 MHz to solve the problem, depending on the operating and initial conditions. In order to optimize the CPU time we used Powell's hybrid method to solve the corresponding steady-state balances (12). Moreover, the Fortran code was rearranged to solve the model in sequential stages. First the system of nonlinear equations for the global concentration of monomer ([*M*]) and global concentration of radicals ($\lambda_{0,0}$) for all cells in a zone is solved. With those values as data, the values for the global concentration of polymer ($\mu_{0,0}$) are calculated for all cells in a zone. Afterwards, values for $\mu_{0,2}$ and $\lambda_{0,2}$ are assumed so that $\mu_{0,1}$ and $\lambda_{0,1}$ may be calculated in an iterative process that continues until all four values converge for all the cells in the zone. Finally, $\mu_{1,0}$ and $\lambda_{1,0}$ are calculated directly at all cells using the previously calculated moments as data. These last two values are used to calculate the number of branches present in the molecules. Arbitrary suitable values were given to the model variables to start the resolution. The required CPU time to solve the entire reactor drops to 5–10 minutes by means of these strategies.

EXPERIMENTAL INFORMATION

A set of twenty eight different experimental runs were collected from two of Repsol's autoclave reactors for model validation purposes. The samples cover a wide range of polymer grades. Ten samples correspond to low density polyethylenes and the remaining ones correspond to EVA copolymers, containing between 5 and 40% w/w vinyl acetate. Several different peroxide initiators out of a total of eight were used in any given run. These initiators were fed in several places along the reactor. Cold gas was also fed to the reactor in different positions at temperatures ranging from 20 to 60°C. Operating pressures ranged from 1200 to 1800 kg/cm^2. The desired operating temperature at each zone was reached by controlling the initiator injection rate. Propane was the only modifier used, at a level of up to 15% w/w in the cold feed.

Molecular weight distributions (MWD) of product samples were analyzed by Size Exclusion Chromatography (SEC) in a Waters 150C equipment, using TCB as solvent and 0.04 wt% of Irganox 1010 as stabilizer at 145°C. The operating conditions were as follows: flow rate 0.7 mL/min, sample concentration 5 mg/mL and injection volume 150 μL. The resulting measured average molecular weights are shown in the **Results** section.

PARAMETER ADJUSTMENT

The kinetic constants for the decomposition of the different initiators were obtained from manufacturer information. Their preexponential factors (A) range from 1×10^{12} to 1×10^{17} s^{-1} and their activation energies (*E*) range from 26000 to 38000 cal/mol. While the mixing model only requires information about the ratio of propagation constant to termination constant, the present moment model needs the absolute values of those constants. The propagation constant was selected from the literature (13). No adjustment was performed on this particular constant. Then, the kinetic constant for the termination step was adjusted to match conversions calculated with the moment model with those obtained with the mixing model. The latter were known to match well the industrial reactor values. In this way our moment model output becomes compatible with the previous mixing model. Other kinetic constants used result from an adjustment of the parameters of some of the former Repsol's empirical correlations to improve model predictions following a successive stage procedure. First, empirical kinetic correlations for transfer to propane and to vinyl acetate were adjusted to match experimental and calculated number-average molecular weight at the copolymerization reactor exit. Finally, the transfer to polymer empirical correlation was adjusted to improve the agreement between experimental and calculated weight-average molecular weight at the reactor exit for both polyethylene and copolymer. From the twenty-eight experimental runs available, a total of fifteen polymers, including five polyethylenes and

Table 1. Adjusted Kinetic Constants at the Temperatures of the Sample Runs.

Kinetic constant (s–L–mol)	T = 190°C	T = 250°C
Termination by combination (k_{tc})	2.500×10^7	3.600×10^7
Peroxide initiation (k_c)	1.288	1.612
Thermal degradation (k_{tdt})	29.00	318.0
Chain transfer to solvent (k_{trs})	12.16	65.80
Chain transfer to monomer (k_{trm})	4.190	15.70
Chain transfer to polymer (k_{trp})	42.30	125.0

ten EVA copolymers, were used for the adjusting process. The remaining runs were used to check the predictive capability of the adjusted model.

Table 1 shows the values of the adjusted constants at two temperatures. These temperatures correspond to the ones used in the examples shown later in the paper. The values fall within the range of published data (7). The ratio $k_p/k_t^{1/2}$ compares well with published data on this particular industrial process (14). As usual in this type of work, the adjusted parameters are valid for the particular design of the considered reactors, at operating conditions within the range of those used to produce the polymers employed in the adjusting process. Other reactors, or operating conditions beyond the range considered, would most likely require different values for the parameters. In that case a new adjusting process would be necessary.

RESULTS AND DISCUSSION

Results are presented below that show the validity of the coupling between the mixing and moment models. Detailed calculations on two example simulations for a typical autoclave reactor are discussed. Moment model predictions along the reactor are also shown, which helps to elucidate some features of the industrial system behavior. Finally, a comparison between calculated and experimental product properties is performed.

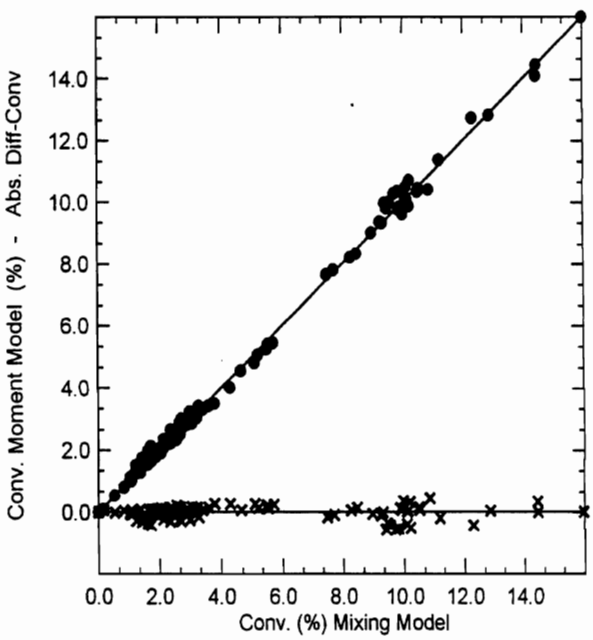

Fig. 2. Moment model and Mixing model conversions at the exit of each one of the reactor zones. (•) Moment model conversion, (×) Absolute difference between both model conversions.

As stated in previous sections, some of the simplifying assumptions present in the mixing model were dispensed with in the moment model. In consequence we considered necessary to check the compatibility of the results common to the two models. At a first stage the match between conversion results obtained with both models was examined. *Figure 2* shows the conversion prediction of one model against the prediction of the other one, at the end of each zone of the reactor for the twenty eight runs employed in this work. Points are very close to the 45° straight line shown in the figure, which indicates good agreement between the two models. This is also evident from the plot of the absolute difference between both predicted conversions, which are all very close to zero. This indicates that releasing the quasi-steady state hypothesis and using the rigorous monomer and radical balances with absolute values for the propagation and termination reactions does not affect the conversion predictions. It should be pointed out that the mixing model predictions on conversion matched well the experimental data, as discussed in a previous work (1). As conversion is related to initiator decomposition into radicals, and the heat of polymerization is related to propagation reaction rate, the mixing model results on temperature and initiator concentration at each cell may be used as valid data for the moment model.

Two example simulations were performed for an autoclave reactor with features that resemble those found in industrial reactors. One simulation was performed for the polymerization of ethylene (PE-B), and the other one for the polymerization of ethylene-vinyl acetate (EVA-B). In the examples, a baffle divides the reactor into a top zone and a bottom zone. Agitation is provided by a shaft with two paddles, one at the top of each zone. *Figure 1* schematically shows the flow pattern in any of the zones. The volume of the top zone is 274 m^3, and 54 m^3 for the bottom one. For modeling purposes each zone is divided into 30 wall cells and 30 shaft cells, adding up to 60 cells in each zone. Fresh gas and initiator are fed at cell 14 at the top zone. At the bottom zone no gas is fed, but there is a single initiator injection at cell 6. The operating conditions are indicated in *Table 2*. The reactor operates at two thermal levels and at constant pressure. The gas

Table 2. Operating Conditions for Example Simulations.

RUNS	Zone	T_{set} (°C)	P (kg/cm²)	FG (kg/h)	VA (% w/w)	S (Mw = 42) (% w/w)	Initiator (mol/h)
PE-B	Top	190	1500	14000	—	7.5	3.675
	Bottom	250	1500	—	—	—	0.504
EVA-B	Top	190	1500	10000	30	2.5	1.152
	Bottom	250	1500	—	—	—	0.252

Table 3. Model Results for Example Simulations.

RUNS	Zone	$Conv_{out}$ (%)	Mn_{out}	Mw_{out}	Mz_{out}	Ln_{out}	Mw/Mn
PE-B	Top	11.1	20215	89005	248655	0.940	4.4
	Bottom	4.40	14848	77626	238706	0.567	5.23
EVA-B	Top	10.6	22775	71640	164792	1.020	3.14
	Bottom	5.70	17063	63278	160292	0.660	3.71

feed contains vinyl acetate in the EVA example. In both examples a chain transfer agent is fed together with the gas. Kinetic information used in these examples is presented in *Table 1*.

Table 3 presents conversion, molecular weights and long-chain branching indexes calculated at the exit of each zone. Total conversion is about 16% for both examples, a typical value for a two-zone reactor. The largest monomer consumption occurs at the top zone, which is the one with largest residence time. Molecular weights are higher at the top zone, mainly because here the reactor operates at a lower temperature at which degradation reactions are negligible compared to propagation and termination by combination reactions. Moreover the kinetic constant for the first initiator decomposition is lower, giving more time for the molecules to grow. Weight average molecular weights for the EVA-B were lower than those for the PE-B run, while number average molecular weights were similar for both runs. In the case of EVA, VA acts as chain transfer agent which favors lower molecular weights. A polydispersity of 5.2 was obtained for PE-B while a lower value of 3.7 was obtained for EVA-B; this follows observed experimental trends. With respect to long-chain branching indexes, values at the reactor exit are of the same order of those reported as reasonable in the literature (5).

Figure 3 shows a comparison between the concentrations of initiator, radicals and polymer along the reactor wall for the two example calculations. Wall and shaft cells at the same axial position are identified with the same index "*k*." Cells have been numbered consecutively, so any cell with a number higher than 30 belongs to the second zone. It should be kept in mind that both gas and initiator are fed at the same positions for both simulations. There is a sharp increase in the initiator concentration at the two injection points, wall cells 16 and 36. There is also an increase when changing from wall cell 30 to wall cell 31, that is, when changing zones. This is due to the different initiator conditions in the two reactor zones. The concentration of radicals closely follows the behavior of the concentration of initiator, as expected. The concentration of polymer tends to increase steadily, following the conversion levels. The analysis of the two example simulations shows that the model predicts reasonable values for molecular parameters and reactor performance.

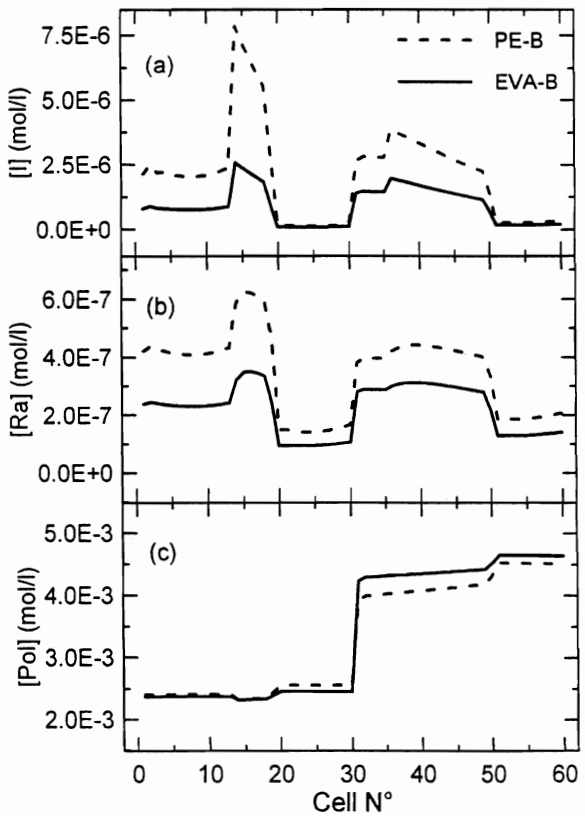

Fig. 3. Concentrations for runs PE-B and EVA-B vs. cell number. (a) Total initiator concentration. (b) Global radical concentration. (c) Global polymer concentration.

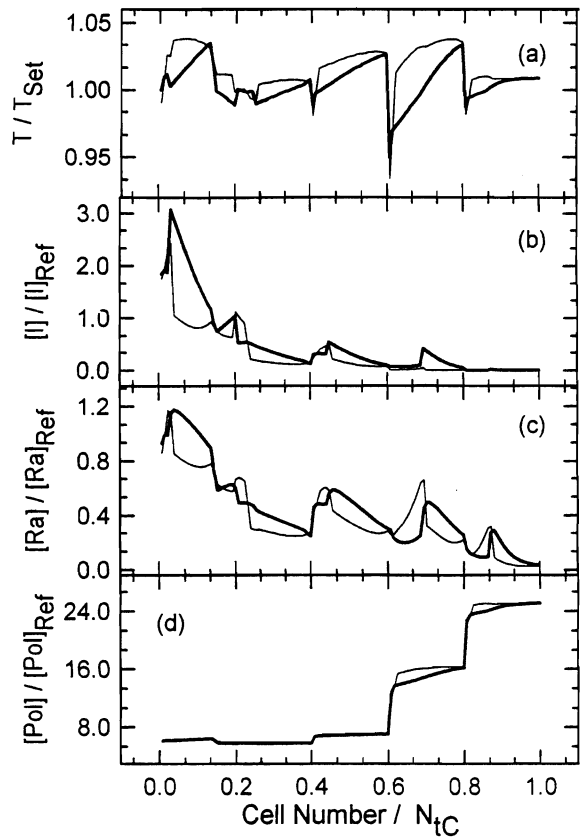

Fig. 4. Temperature and concentrations for run PE-1 vs. Relative Cell Number. (a) Temperature divided by the set temperature for PE-1 at the corresponding zone. (b) Total initiator concentration. (c) Global Radical Concentration. (d) Global polymer concentration. (Concentrations are referred to arbitrary values representative of the order of magnitude in each case.)

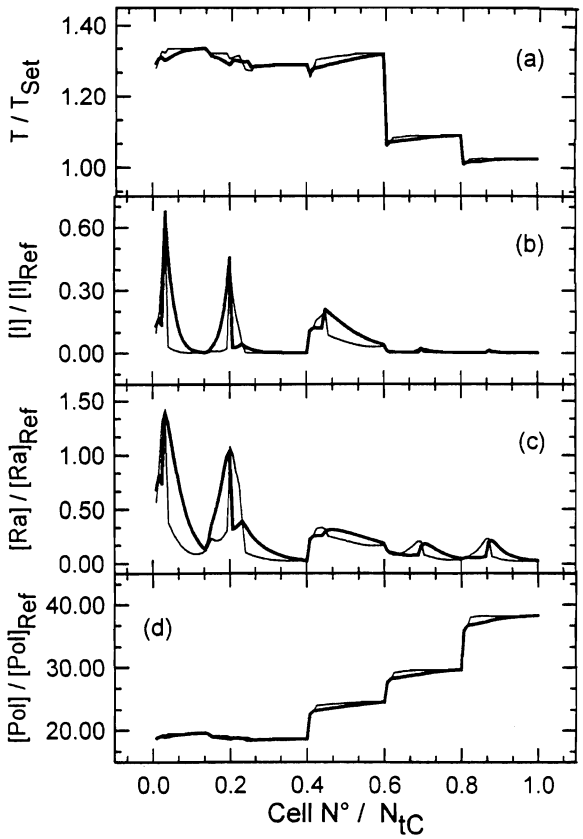

Fig. 5. Temperature and concentrations for run PE-2 vs. Relative Cell Number. (a) Temperature divided by the set temperature for PE-1 at the corresponding zone. (b) Total initiator concentration. (c) Global Radical Concentration. (d) Global polymer concentration. (Concentrations are referred to arbitrary values representative of the order of magnitude in each case.)

For the actual reactors, two polyethylenes (PE-1 and PE-2) and two EVA copolymers (EVA-7 and EVA-17) were selected to show the main results of the moment model coupled with the mixing model along the reactor cells. The properties of these polymers are representative of the range of molecular properties produced in the studied reactors.

Figures 4 to *11* show dimensionless axial profiles of temperature, total concentrations of initiator, radical and polymer, long chain branching, and average molecular weights near the reactor wall and near the reactor shaft. Thick lines correspond to wall profiles while thin lines correspond to shaft profiles. The axial position is measured as the ratio between the cell number and the total number of cells. For a given cell the radial profiles are represented by the values at the reactor wall and center. All values are reported relative to a "reference" as detailed in the figures. The reference for each parameter has the same value for all figures.

Let us first analyze the main features of the polyethylene profiles. For PE-1, the temperature profile has values near one because the actual values are divided by the set temperature of each zone for this same run (*Fig. 4a*). Note that in general a gap between 25 and 60°C exists between successive zones. At every point where an initiator injection occurs a sharp jump in total initiator concentration is observed followed by its consumption (*Fig. 4b*). This change is followed by the temperature profile, in the opposite direction. This is because the addition of initiator causes an increase in the concentration of free radicals (*Fig. 4c*), which in turn fuels the propagation reaction, and the latter is the main responsible of heat generation. These related effects allow the control of the cell temperature through the flow rate and position of the initiator injections. In these reactors the injection rates were calculated using the mixing model so as to maintain the temperature as close as possible to its set value. We can see in *Fig. 4* that this objective has been achieved, as the difference between the cell temperature and the set temperature for the zone is always less than 5%.

When comparing the wall and shaft temperature at the same axial point, we can see that shaft temperature is always higher. This leads to a faster initiator consumption near the shaft. This combination of conditions at the shaft would lead to a lower molecular

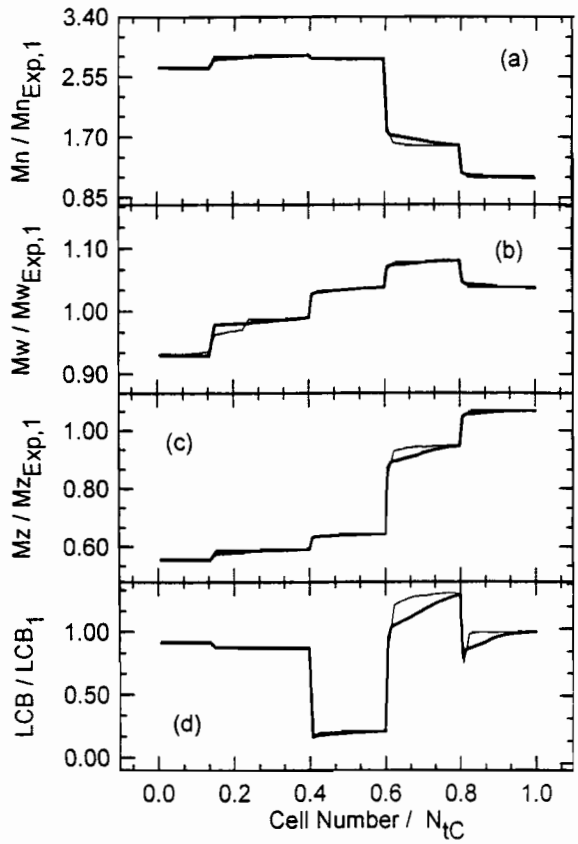

Fig. 6. Average molecular properties for run PE-1 vs. Relative Cell Number. (a) Number average molecular weight. (b) Weight average molecular weight. (c) z average molecular weight (d) Number average long chain branching/1000C. (Molecular weights are reported relative to the corresponding experimental value for PE-1 while long chain branching is reported relative to the calculated value for PE-1 at the reactor exit.)

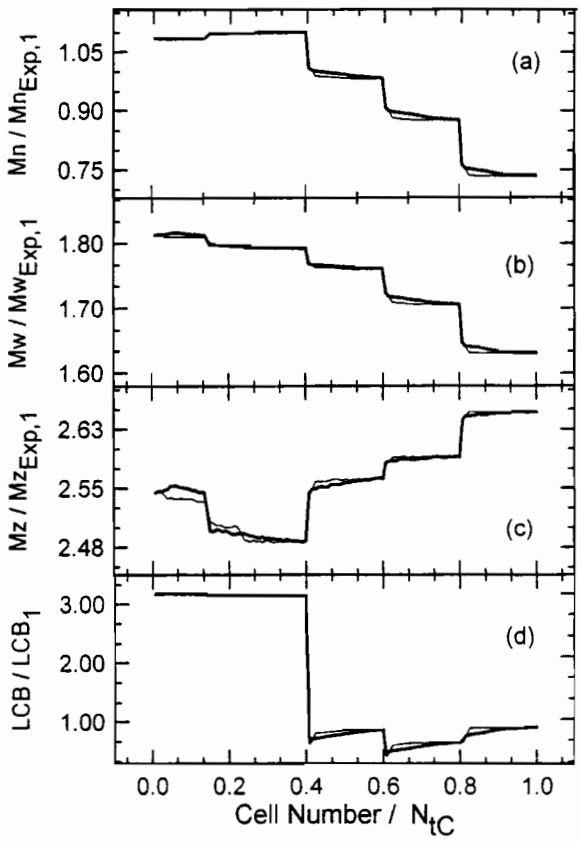

Fig. 7. Average molecular properties for run PE-2 vs. Relative Cell Number. (a) Number average molecular weight. (b) Weight average molecular weight. (c) z average molecular weight (d) Number average long chain branching/1000 C. (Molecular weights are reported relative to the corresponding experimental value for PE-1 while long chain branching is reported relative to the calculated value for PE-1 at the reactor exit.)

weight. When considering polymer production (*Fig. 4d*), polymer concentration increases from one zone to the next, this trend being most evident at the last zones where temperatures are higher. In this case no significant difference between wall and shaft values was predicted.

In the case of PE-2 (*Fig. 5a*) the reactor was operated at temperatures approximately 30% higher in the top zones than when producing PE-1, while the operating temperatures of bottom zones were similar to case PE-1. This indicates that the temperature gap between the top and bottom area was lower than for PE-1. Less initiator concentration was necessary at each cell to maintain the desired temperature (*Fig. 5b*). Obviously, another set of initiators must have been used to be able to operate at higher temperatures and at these concentration levels. Free radical profiles follow the initiator profile features (*Fig. 5c*). Polymer molar concentrations (*Fig. 5d*) are higher than for PE-1. This may be expected since at higher temperatures more initiator radicals will be present, so more polymer molecules will be formed.

With respect to molecular weights, results for PE-1 and PE-2 are shown in *Figs. 6* and *7*, respectively. The largest polymer molecules are produced in the first portion of the reactor where temperatures are kept lower. At these temperatures thermal degradation is not significant, which allows propagation to proceed for a longer time. The set temperature for the first zone in PE-1 was lower than the corresponding one in PE-2. Then, we should expect higher *Mn* in the first case; model results (*Figs. 6a* and *7a*) are in agreement with this interpretation. Overall, a decrease in *Mn* is observed along the reactor path for both polymers accompanying the rise in temperature.

When analyzing weight average molecular weights (*Figs. 6(b)* and *7(b)*), an increase along the reactor path is observed for PE-1. Inversely, *Mw* tends to decrease along the reactor in the case of PE-2, with starting and ending *Mw* values that are always higher than the corresponding ones for PE-1. PE-1 is obtained in heterogeneous conditions in the top zones, and homogeneous conditions in the bottom zones. This means that the transfer to polymer rate constant

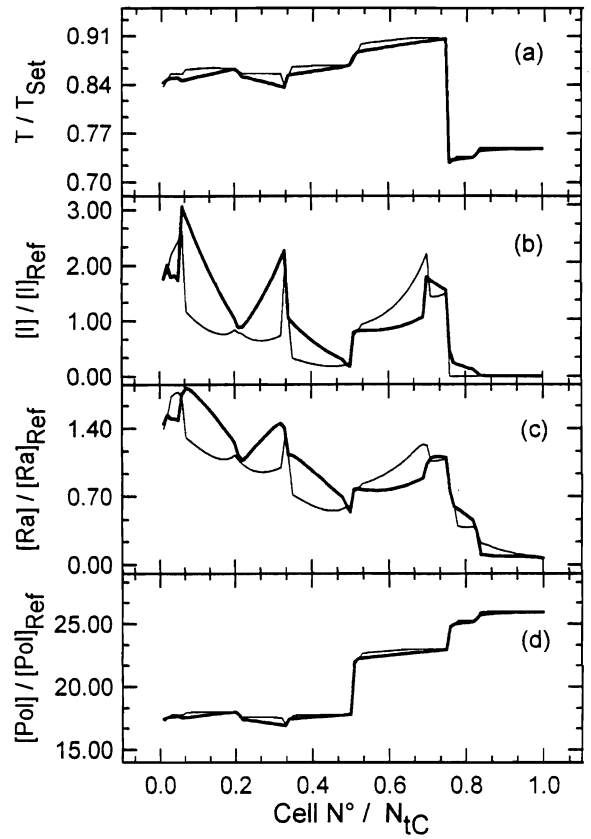

Fig. 8. Temperature and concentrations for run EVA-7 vs. Relative Cell Number. (a) Temperature divided by the set temperature for PE-1 at the corresponding zone. (b) Total initiator concentration. (c) Global Radical Concentration. (d) Global polymer concentration. (Concentrations are referred to arbitrary values representative of the order of magnitude in each case.)

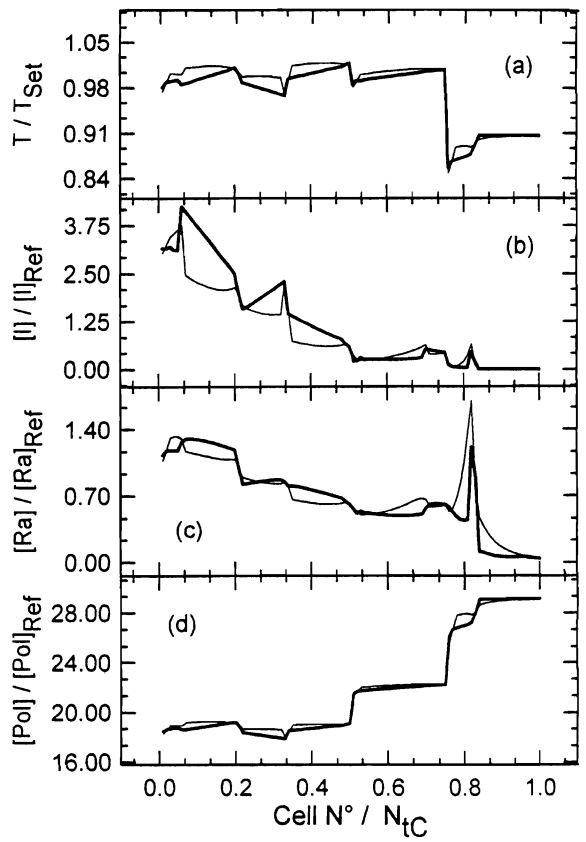

Fig. 9. Temperature and concentrations for run EVA-17 vs. Relative Cell Number. (a) Temperature divided by the set temperature for PE-1 at the corresponding zone. (b) Total initiator concentration. (c) Global Radical Concentration. (d) Global polymer concentration. (Concentrations are referred to arbitrary values representative of the order of magnitude in each case.)

tends to increase along the reactor path because of the change in the number of phases. Since thermal degradation and transfer to polymer reactions also become more important as temperature increases, this leads to an increase in polydispersity, as observed. Polyethylene PE-2, on the other hand, is obtained under homogeneous conditions. As reported in the literature (15), this tends to result in higher molecular weight material. The decrease along the reactor path should not be surprising because of the complex dependence of k_{trp} on various process variables. The presence of one or two phases are accounted for in our models through the use of an empirical correlation for transfer to polymer kinetic rate constant (k_{trp}). This correlation is a non-trivial function of not only temperature and pressure but also conversion and the polymer structure. As a result k_{trp} may be up to an order of magnitude lower for runs conducted in two phases. In the considered polyethylenes, the reactor is operated at low k_{trp} conditions for PE-1 while for PE-2 the reactor is operated at high k_{trp} conditions in the top zones switching to low k_{trp} conditions in the last zones, lowering *Mw*. *Mz* (*Figs. 6c* and *7c*) accompanies *Mw* variations in each case. Note that in the PE-2 run higher propane content was needed to control molecular weight.

Results on long chain branching are shown in *Figs. 6d* and *7d*. No significant difference is predicted between wall and shaft values. The model predicts that for one-phase operation the resulting polyethylene has many more branches in the first zone than the polymer obtained in two phases. This is to be expected from the higher k_{trp} in one-phase operation.

We analyze two copolymer grades, EVA-7 (*Fig. 8*) and EVA-17 (*Fig. 9*) that correspond to high and low vinyl acetate content copolymers, respectively. For copolymers, temperatures at the top zone are close to the ones used to produce PE-1, but in the bottom zone the temperature is much lower than the maximum temperatures used for polyethylenes. The operating temperatures for these two EVA copolymers are similar, but they are somewhat higher for EVA-17 as can be seen from *Figs. 8a* and *8b*. Initiator and radical concentrations variations (*Figs. 8b*, *8c*, *9b* and *9c*) are related in a similar way as in the polyethylene cases. Copolymer concentration increases along the reactor

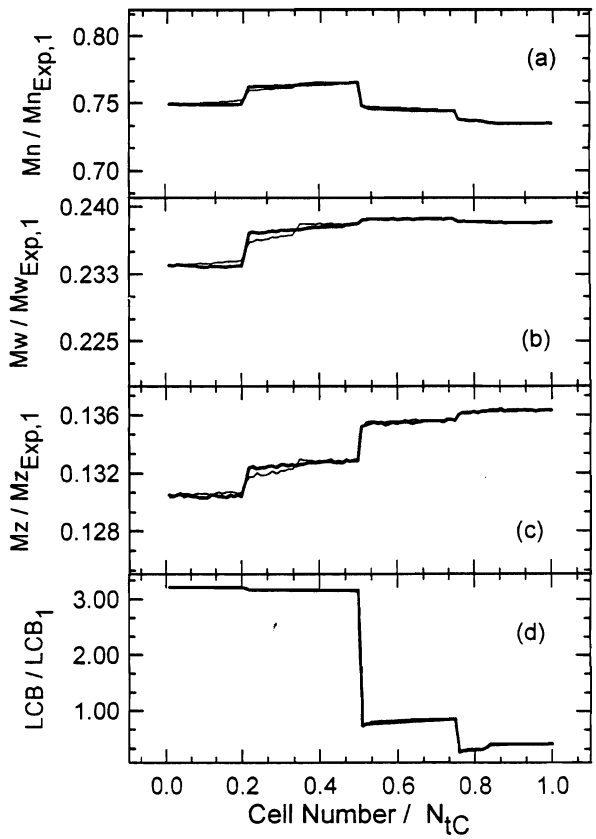

Fig. 10. Average molecular properties for run EVA-7 vs. Relative Cell Number. (a) Number average molecular weight. (b) Weight average molecular weight. (c) z average molecular weight (d) Number average long chain branching/1000 C. (Molecular weights are reported relative to the corresponding experimental value for PE-1 while long chain branching is reported relative to the calculated value for PE-1 at the reactor exit.)

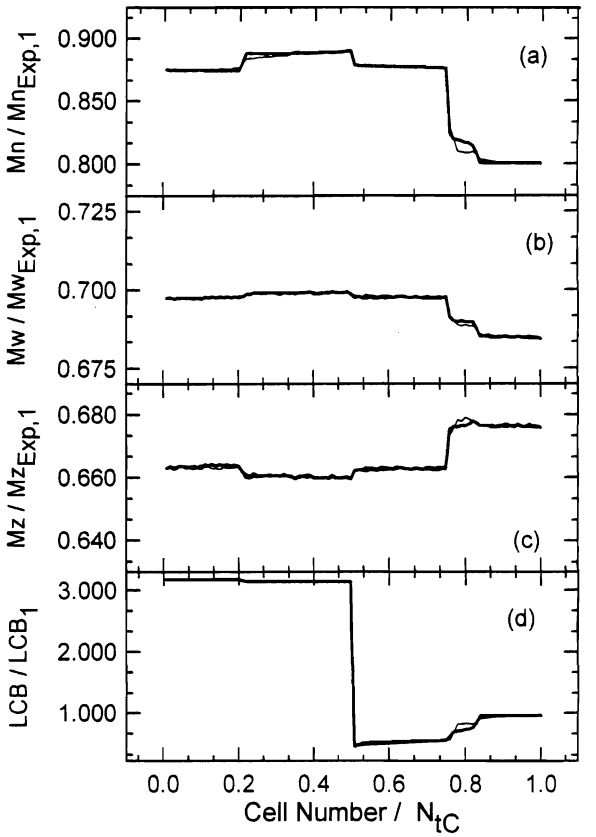

Fig. 11. Average molecular properties for run EVA-17 vs. Relative Cell Number. (a) Number average molecular weight. (b) Weight average molecular weight. (c) z average molecular weight (d) Number average long chain branching/1000 C. (Molecular weights are reported relative to the corresponding experimental value for PE-1 while long chain branching is reported relative to the calculated value for PE-1 at the reactor exit.)

path according to the expected increase in conversion (*Figs. 8d* and *9d*). In general the differences between concentration at the wall and shaft at the same level in the reactor do not translate into the corresponding molecular properties. *Figures 10a* to *10c* and *11a* to *11c* show molecular weight profiles for the two EVA copolymers. For these copolymers, the variations along the reactor are less evident than for the polyethylene case. In general copolymers obtained with high VA content, for example EVA-7, need less propane to control the molecular weight, since both VA and propane act as transfer agents. In general copolymers obtained with low VA contents, like EVA-17, show higher molecular weights and polydispersity than those obtained in the upper level of VA range. *Figures 10d* and *11d* show the corresponding long chain branching profiles. The figures show that long chain branching diminishes along the reactor. For the cases shown, the level of branching is similar to that present in polyethylenes.

Figures 12 and *13* compare experimental and calculated average molecular weights at the reactor exit for polyethylenes and EVA copolymers respectively. They also show long-chain branching predictions, for which no experimental data were available. The model follows well the observed experimental trends for all average molecular weights and gives good estimates of both number and weight average molecular weights, within experimental error. Polymers with the highest *Mw*, which are reaching the gel point, posed the greatest difficulty in the model calculation, evidenced in larger CPU times. The predictions of *Mz* are worse in magnitude but in general they also follow the experimental trends for both homopolymer and copolymer. No parameter adjustment was done to optimize *Mz* predictions.

In the case of polyethylene the empirical relationships for transfer to propane were used as originally provided by Repsol, without performing any parameter tuning to improve *Mn* predictions. The average relative error in *Mn* was less than 8%. For the EVA copolymers an extra parameter adjustment was done on the transfer to propane and to vinyl acetate kinetic constants. The average relative error in *Mn* was about

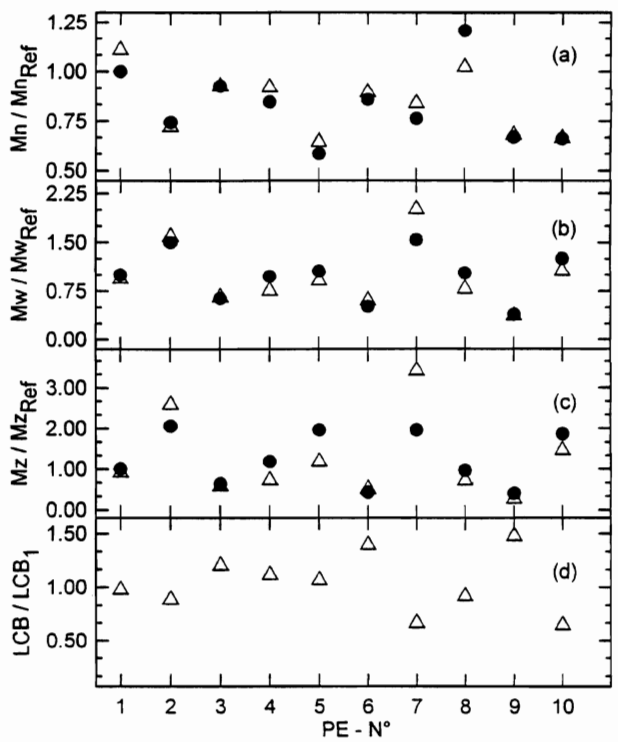

Fig. 12. Calculated (△) and experimental (●) average molecular properties for different polyethylenes. (a) Number average molecular weight. (b) Weight average molecular weight. (c) z average molecular weight (d) Number average long chain branching/1000 C. (Molecular weights are reported relative to the corresponding experimental value for PE-1 while long chain branching is reported relative to the calculated value for PE-1 at the reactor exit.)

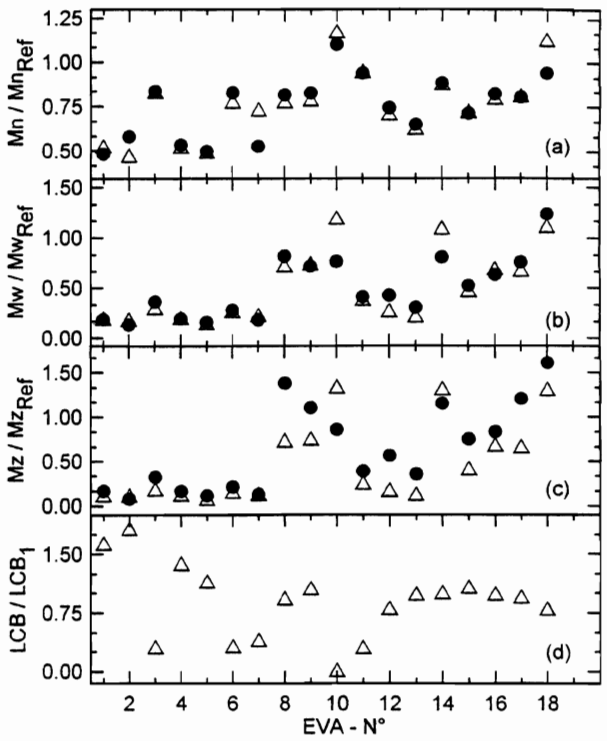

Fig. 13. Calculated (△) and experimental (●) average molecular properties for different copolymers. (a) Number average molecular weight. (b) Weight average molecular weight. (c) z average molecular weight (d) Number average long chain branching/1000C. (Molecular weights are reported relative to the corresponding experimental value for PE-1 while long chain branching is reported relative to the calculated value for PE-1 at the reactor exit.)

8% for the high VA content copolymer descending to a 5% error for the lower vinyl content copolymers.

To optimize the *Mw* prediction some tuning of the transfer to polymer kinetic parameter was done. The average relative error in *Mw* was about 15% for the polyethylenes, and less than 18% error for the lower vinyl content copolymers. These average errors were calculated without excluding any case.

Measured MFI compared with predicted MFI using calculated molecular properties are plotted in *Fig. 14*. It may be observed that results are very good when using molecular properties calculated by the model. Please note that we have used different correlations to predict polyethylene MFI and EVA copolymer MFI.

CONCLUSIONS

A mathematical mixing model that describes autoclave polymerization reactors for low density polyethylene production was generalized to include predictions on molecular properties. The original mixing model could predict conversions, initiator consumption, global concentrations of monomer, solvent, and number average molecular weight at any position along the reactor. The moment model presented in this work may calculate those same quantities, plus radical and polymer concentrations, higher order moments and average molecular properties along the reactor at wall and shaft positions. Those extra properties are *Mw*, *Mz*, long chain branching index and melt flow index.

The model is able to manage incoming and outgoing flow of radicals in the cells because the usual quasi steady state approximation is not used.

We found improved convergence by solving the moment model equations as a steady state problem, even though it is ill-conditioned, rather than solving the nonsteady state problem from a suitable starting point until reaching the stationary state. Considerable reduction in required CPU time was achieved by solving the problem in successive stages.

The model predictions agree well with experimental trends for *Mn*, *Mw* and *Mz* not only for polyethylene grades but also for EVA copolymers. When considering the absolute values of those parameters, the gap between theory and experiment is more evident for polymers obtained under two-phase conditions. In general, model predictions reflect the fact that the polymer is approaching the gel point. Predictions for MFI also agree well with experimental data.

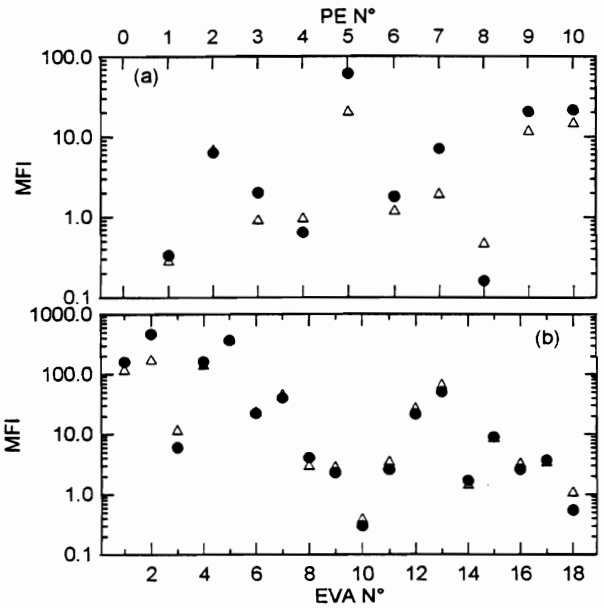

Fig. 14. Calculated and experimental MFI. (a) Polyethylene, (b) Copolymers. (•) Experimental, (Δ) From calculated molecular properties.

ACKNOWLEDGMENTS

The Repsol authors would like to acknowledge the contribution of A. Gilchrist and R. A. Jackson of ICI in providing a simple stirring current model from which the more elaborate model was developed. We are indebted to M. Aroca (Repsol) for the molecular weight measurements. The PLAPIQUI authors would like to acknowledge CONICET for financial support. We thank Dr. Pedro E. Ugrin for his efforts in data collection.

NOMENCLATURE

f = Efficiency for radical formation from a peroxide initiator.
F_G = Cold feed volumetric flow to shaft and wall "k" cells.
F_{Gks} = Cold feed volumetric flow to shaft cell "k."
F_{Gkw} = Cold feed volumetric flow to wall cell "k."
F_{Sk} = Shaft axial volumetric flow from shaft cell "k."
F_{Uk} = Radial volumetric flow from shaft cell "k" to wall cell "k."
F_V = Generic Volumetric flow.
F_{Wk} = Wall axial volumetric flow from wall cell "k."
F_{Zk} = Radial volumetric flow from wall cell "k" to shaft cell "k."
I = Peroxide initiator.
k_c = Kinetic constant for peroxide initiation.
k_p = Kinetic constant for propagation reaction.
k_{tc} = Kinetic constant for termination by combination reaction.
k_{tdt} = Kinetic constant for termination by thermal degradation.
k_{trm} = Kinetic constant for transfer to monomer reaction.
k_{trp} = Kinetic constant for transfer to polymer reaction.
k_{trs} = Kinetic constant for transfer to solvent reaction.
LCB = Number average long chain branching/ 1000 C.
M = Global monomer.
$\bar{M}_{mon}$ = Monomer average molecular weight.
MFI = Melt flow index.
Mn = Number-average molecular weight.
Mw = Weight-average molecular weight.
Mz = z-average molecular weight.
$Ncell$ = Total number of cells in which a zone is divided.
Nin = Number of entrances to a cell.
NIT = Total number of peroxide initiators.
$Nout$ = Number of exits from a cell.
NST = Total number of solvents.
$P_i(x)$ = Polymer with "i" branches and "x" monomer units $i = 1..\infty$, $x = 1..\infty$.
$R_1(0)$ = Linear radical without monomer, produced by peroxide decomposition.
$R_i(x)$ = Radical with "i" branches and "x" monomer units $i = 1..\infty$, $x = 0..\infty$.
$[Ra]$ = Total radical concentration.
S = Solvent.
t = Time.
V = Volume.
VA = Vinyl-Acetate.

Greek Symbols

$\delta_{i,j}$ = Kronecker's Delta.
$\lambda_{m,n}$ = m^{th}, n^{th} moment of radical concentration distribution.
$\mu_{m,n}$ = m^{th}, n^{th} moment of polymer concentration distribution.

Subscripts and Superscripts

in = Input.
G = Cold gas feed.
i = Input/output counter.
k = Generic cell counter.
ks = Shaft cell counter.
kw = Wall cell counter.
out = Output.

REFERENCES

1. A. López-Rodríguez, J. J. Pedraza, and B. del Amo, *Computer Chem. Eng.*, **20**, S1625 (1996).
2. G. Donati, M. Gramondo, E. Langianmi, and L. Marini, *Ing. Chim. Ital.*, **17**, 88 (1981).
3. C. Georgakis and L. Marini, "The Effect of Mixing on the Steady-State and Stability Characteristics of LDPE Vessel Reactors," in *Chemical Reaction Engineering*, A. C. S. Symp. Ser., **196**, 591, Boston (1982).

4. L. Marini and C. Georgakis, *AIChE J.*, **30**, 401 (1984).
5. W.-M. Chan, P. E. Gloor, and A. E. Hamielec, *AIChE J.*, **39**, 111 (1993).
6. R. C. M. Zabisky, W.-M. Chan, P. E. Gloor, and A. E. Hamielec, *Polymer*, **33**, 2243 (1992).
7. A. Brandolin, M. H. Lacunza, P. E. Ugrin, and N. J. Capiati, *Polym. Reac. Eng.*, **4**, 193 (1996).
8. H. M. Hulburt and S. Katz, *Chem. Eng. Sci.*, **19**, 555 (1964).
9. S. Katz and G. M. Saidel, *AIChE J.*, **13**, 319 (1967).
10. C. H. Chen, J. G. Vermeychuck, S. A. Howell, and P. Ehrlich, *AIChE J.*, **22**, 463 (1976).
11. C. W. Gear, *Numerical Initial Value Problems in Ordinary Differential Equations*, Prentice-Hall, Englewood Cliffs, N. J. (1971).
12. M. J. D. Powell, "A Hybrid Method for Non-Linear Equations," *in Numerical Methods for Non-Linear Algebraic Equations*, P. Rabinowitz, ed., Gordon and Breach, London (1970).
13. P. C. Lim and G. Luft, *Makromol. Chem.*, **184**, 849 (1983).
14. J. J. Pedraza, A. López, and B. del Amo, *2nd IUPAC-Sponsored International Symposium on Free Radical Polymerization: Kinetics and Mechanisms, Preprints Book*, pp. 43–46, Santa Margherita Ligure, Italy (1996).
15. V. Bogdanovic and J. Srdanovic, *J. Appl. Polym. Sci.*, **31**, 1143 (1986).